The November 2021 Fin (SE Zagros, Iran) doublet earthquakes of reverse faults in a transpressional tectonic regime

Majid Nemati (nematimajid_1974@uk.ac.ir)
Shahid Bahonar University of Kerman

Research Article

Keywords: Fin, Earthquake, acceleration, mechanism, Coulomb

Posted Date: March 17th, 2022

DOI: https://doi.org/10.21203/rs.3.rs-1314781/v1

Abstract

Doublet earthquakes with magnitudes of 6.2 (12:07) and 6.3 (12:08 GMT) on December 14, 2021 struck the SE Zagros in the range of the Mountain Frontal Fault (MFF) in south of Iran. By combining and processing the records of the seismic networks, mechanism of some of background seismicity and the aftershocks were solved and Coulomb stress maps of epicentral area were drawn. Reverse mechanism with a small strike slip component in some earthquakes were dominant, if north dipping E-W oriented plane is the active plane. Statistical investigation of the earthquakes parameters demonstrated that no considerable seismic gap was seen before the first mainshock. The 12:08 Fin earthquake, like other Mountain Frontal Fault dependent earthquakes, is associated with the probable development of anticlines in its vicinity, which is accompanied by a faulting process in and around the core. A small area of fractures with a maximum length of hundred meters and few centimeters opening were seen in the nearest main road. No coseismic mature fault related to this magnitude was observed in prospecting in high quality satellite images. The coulomb stress field revealed that the second shock and majority of aftershocks happened in area of increased stress produced by the first mainshock and second earthquake, respectively. Dimension and strike of coseismic rupture of the second event are estimated ~50 km and near ENE-WSW, respectively using both aftershocks elongation and special-temporal diagram of micro earthquakes. Northward directivity was seen for both shocks in their accelerograms of northeast and south of the epicenters. If MFF fault is supposed as causative fault for the second shock, second rupture was probability propagated from the south to the north, unilaterally. Based on northward dipping of the MFF, the rupture of second event could propagate from shallow depth (10 km, hypocenter) toward deep area (12 km, centroid) of the fault along N-S direction. If causative faults of the shocks are back thrusts, the first rupture should be south dipping, and propagate from depth (20 km, hypocenter) toward surface (13 km, centroid) in N-S direction.

Introduction

Fin doublet earthquakes happened in the south Zagros related to the (MFF). Location of the two mainshocks are in north of Gianu anticline and related segment of MFF (Institute of Geophysics, the University of Tehran, IGUT). The highest intensity of the earthquake was reported in Fin and Geno villages in NE of Bandar-e Abbas city, capital of Hormozgan province. The quakes and related aftershocks killed one person and the rock falls and small landslides happened in neighboring mountains around the epicenters. Folding in the epicental area of the earthquake is similar to folds in the neighborhood or on the hanging wall of the mountain frontal fault segments (Berberian 1995) (Table-1 and Fig. 1).

Table-1. Source parameters of 2021/11/14_12:07 and 12:08 Fin earthquakes.

	Y	*MD*	*HM*	*S*	*X(°E)*	*Y(°N)*	*Hypocenter (km)*	*Centroid (km)*	*St(°)*	*D(°)*	*R(°)*	*Magnitude*	*Reference*
1	2021	1114	1207	4.3	56.084	27.568	19.5	12.0	94.00	34.00	89.00	MN 6.2	IRSC
2					56.075	27.668	14.0	-	-	-	-	ML 6.3	IIEES
3					56.065	27.721	5.6	-	289.00	85.00	101.00	MW 6.0	USGS
5					-	-	-	-	252.29	37.70	64.96	-	here
6	2021	1114	1208	0	56.174	27.536	10.0	13.0	275	66	98	MN 6.3	IRSC, GCMT

MFF is recognized as the nearest neighbor fault to the epicentral area of these earthquakes. This fault is assumed as boundary between simply folded belt and Persian Gulf (parts of Zagros). This fault is extended for about 1350 km composed of discreet segments with length of 15-115 km. Vertical uplift along this reverse and sometimes buried fault is estimated more than 6 km. MFF is associated with many folds along the discreet segments (Berberian 1995).

Here, the consistency of the processed characteristics of these earthquakes with the processed characteristics about the Zagros tectonic (e.g. Berberian 1995 and Hatzfeld et al. 2010), especially in the vicinity of the mountain frontal fault, has been studied. There are still many challenges regarding the mechanism and rate of absorption of shortening on the active faults in the Zagros. The 2021 Fin earthquake provided a new challenge to investigate the mechanism of earthquake, aftershocks and its relation and Coulomb analysis to illustrate tectonic in the area. This study tries to investigate the Dec. 14, 2021 earthquakes sequences using seismic data.

Seismotectonic settings

GPS data indicates a rate of ~21 mm/year for the convergence of Arabia-Iran in Persian Gulf with ~E10˚N direction (e.g. Vernant et al. 2004). According to seismotectonic of the area, the Zagros seismotectonic province has different behaviors from northeast to southwest that can be divided into several parts: the high Zagros, the simply folded belt and the Zagros foredeep. Geomorphology in the simply folded belt is more

visible in the form of folds. The size and geometry of these folds and their related discreet faults (e.g. MFF) are the result of heterogeneity in rheology of shallow crust in the Zagros (e.g. Berberian 1995).

In Zagros, there is no good agreement between deep microseismicity and bedrock faults (like MFF) as well as surface structures (Figure 1). At least in the middle Zagros in depths, the micro earthquakes concentrate in parallel groups and have no compatibility with the known faults and surface folds (Tatar et al. 2004). The distribution of earthquakes larger than 5.5 indicates that the high Zagros is not active except in the strike slip faults and the folded Zagros is active only in its northern half, close to the high Zagros, and this is mainly related to thrust faults.

Also, the Zagros area is characterized by several seismic and geologic parts separated by right-slip faults from the northwest to southeast. The Zagros large reverse faults are the High Zagros Fault (HZF), the MFF and the Zagros Foredeep Fault (ZFF). Reverse faults are in line with the direction of Zagros range and its folds, and right lateral faults have cut them in the NNW-SSE direction and displaced them in a right lateral manner. Both thrust faults and folds to the southwest of the Zagros range are younger, indicating the geological evolution progress to the southwest (Alavi 2004).

There have been several major earthquakes in the Fin neighboring region. The 2006 Fin and the 1995 (Roustaei et al. 2010) Darab events (Walker et al. 2005) (both with M_W 6.4) related to the mountain frontal fault and the High Zagros fault, respectively (Fig. 1). Except for the northeast of Bandar-e Abbas (Oman line area in NE part of the Fig. 1) with a maximum depth of 50 km (Yamini-Fard et al. 2007), the maximum depth of earthquakes in Zagros reaches 20 km (e.g. Talebian and Jackson 2004; Nissen et al. 2019). Previous studies have shown that earthquakes that occur in the Zagros can also be located within the ~10 km width sedimentary cover (Mcquarrie 2004). Recent studies show that sedimentary cover could also be seismic (e.g. Nemati et al. 2011) including in the Zagros (Hatzfeld et al. 2010).

The mentioned reverse faults are with a northeastern dipping that have been cut by the system of right lateral faults like: Kazerun, Karebas, Sabzpoushan and Sabzevaran faults (Berberian 1995). The Zagros Foredeep fault is the boundary of the Zagros Simply Folded Belt and the Zagros Foredeep. However, new research shows that the rupture of this fault in some places has an outcrop (e.g. Bachmanov et al. 2004).

Data And Methods

High resolution satellite photographs and the Google Earth pictures were used to prospect the earth surface, systematically to find a mature rupture. The aftershocks of this earthquake have not been collected by a compact local seismological network. This study has investigated these earthquakes by combining the seismic data of the seismic network of the IGUT (130 stations), the International Institute of Seismology and Earthquake Engineering of Iran (IIEES) with more than 30 stations (inset map of the Fig. 2). This data was processed with Seisan software (Ottemoller and Havskov 2012) and displayed with GMT (Wessel and Smith 1998) and Power Point software.

The IGUT devices are mainly SS1 Short Periods and the IIEES devices are mostly Broadband Goralp (CMG-3T; www.guralp.com). The Pn and Pg phases were used to processing for farther than 150 km and closer, respectively. Although the event mechanisms were processed using the first polarizations of the compressive P waves using minimum 10 and maximum 47 stations (Fig. 2).

We forced the SEISAN software to solve the mechanisms with maximum 5° freedoms in rotation of the nodal planes. Mechanism determination was hardly solved with azimuthal coverage deficiency. The nearest stations to the epicentral area like JASK, BNB, BNDS, GENO, MZN1 and KHJ1, with pg phases were useful for mechanism determination. The stations with fair azimuthal coverage related to the epicentral area like JASK, LMD1, NGCH, SRVN, BAZ1 and CHBR (www.irsc.ir, www.iiees.ir) helped us to cover the azimuthal gap during focal mechanism solution. They have far distances to the center of the focal sphere and make the nodal planes stable. According to the fact that no long time has been elapsed from the mainshock, ISC has not read polarity of P waves of the seismological stations of the United Arabia Emirate, Kingdom Saudi Arabia, Oman and Qatar countries, yet. Therefore, we have to merge only IGUT and IIEES recorded waveforms. Polarity of stations near to the nodal planes was double checked, because they have more important role in comparisons to the other stations. Polarity these stations could limit degree of freedoms of rotation of nodal planes in focal sphere.

The Origin software (http://www.microcal.com) was used to calculate and display statistical parameters and diagrams of IGUT data (Fig. 3 and 4). Columns of the histograms were set by the Origin software, automatically. All the maps (Fig. 1, 2, 3a and Fig. 5a, b) were produced and plotted by the GMT software (Wessel and Smith 1998).

Contour shake maps and strong motion waveforms were presented in this paper (Fig. 5). We used the “krigging method” (suggested by the software) method to generate the gridded data, which is needed to create contour maps of accelerometer stations in the Surfer software (https://www.goldensoftware.com). Then, the gridded data were read by the software to draw a contour map of acceleration for each earthquake. Peak ground accelerations (PGA) of each station, were interpolated to generate these maps. The rupture directivity can be measured from azimuthal variations in the duration of ground-motion, and the amplitude of the accelerogram waveforms (from Building and House Research Center, BHRC, https://www.bhrc.ac.ir/) recorded at similar distances, preferably in same line with the epicenter. The

substantial unilateral rupture causes constructive interference and increased waveform amplitudes in the forward directivity region, while the separation of the pulses of motion increases the duration of the accelerograms in the backward directivity region (e.g. Nemati et al. 2020). Similar conditions were observed in the waveform of accelerograms on both sides of the MFF in epicentral area in this study.

In recent decades, the phenomenon of interaction of seismic events has been proposed as one of the important characteristics of seismicity that leads us to the occurrence of large earthquakes and aftershocks (Stein 1999). This phenomenon, which occurs as a result of the stress transfer process released by earthquakes, has been studied by various models (e.g. Yazdanfar et al. 2018). In this paper, the Coulomb stress change calculations are performed based the Acada analytical model and using Columbus 3.3 software (Lin and Stein 2004; Toda et al. 2005). In the Akada analytical model, the earth is assumed to be a homogeneous elastic hemisphere, in which the rupture is considered to be a rectangular detachment (Okada, 1992). One of the most common methods is the Coulomb stress change criterion (static stress change), expressed as equation (2-1) (Harris 1998; Stein 1999; King and Cocco 2001).

2-1) $\Delta\delta_f\,(\Delta CFS) = \Delta T + \mu' \Delta\delta_n$

In this equation, Δδf represents the change in rupture stress resulting from the reference fault on the receiver fault, ΔT and Δδn change the shear and normal stress, respectively, and μ the effective coefficient of friction on the receiver fault.

Results

3.1- Seismicity and Mechanism

Figure 2 shows seismicity and mechanism of some background seismicity and aftershocks (Table 1) in epicentral area. IIEES aftershocks are shown with blue symbols in main map of the Figure 2. Upper inset map shows the epicentral area of the earthquake and geological structures (anticline and syncline) in a closer view. Red circles in this map display 272 IGUT aftershocks with M_N>2.5. IIEES aftershocks were relatively located far from the MFF in northern area, while IGUT aftershocks were located nearer to Gianu anticline and the related MFF segment. Station distribution of IGUT and IIEES are displayed with black and gray triangles on lower inset map, respectively.

Table-1. Numerical characteristics of source parameters of the greatest aftershocks and background seismicity around epicentral area. Bolded line is the first mainshock parameters.

	Y	MD	HM	S	X(°E)	Y(°N)	Z	St(°)	D(°)	R(°)	RMS	MN	N S	N P
1	2014	1110	1352	28.1	55.546	26.908	8.1	270.80	31.61	49.26	1.1	5.3	17	47
2	2014	1208	638	17.5	56.211	27.452	14.2	314.66	71.33	31.36	0.5	4.3	17	21
3	2015	125	2011	19.4	56.211	27.403	8.7	68.46	52.84	16.01	0.8	5.0	18	20
4	2015	218	1728	53.1	56.301	27.356	7.3	19.72	82.36	49.57	0.8	4.0	16	10
5	2016	706	2358	26.8	56.432	27.657	16.4	241.38	39.67	26.03	0.5	5.0	23	19
6	2018	1205	2012	36.9	56.246	27.302	13.1	75.23	45.14	84.35	0.9	4.2	27	17
7	2019	617	1332	25.9	55.928	27.484	12.5	258.72	44.04	2.07	0.8	4.3	31	18
8	2020	120	1449	38.3	56.425	27.659	18.4	197.95	40.95	-26.25	0.4	4.3	25	23
9	2020	909	1042	50.5	56.261	27.419	11.3	50.17	78.91	47.01	0.6	4.2	28	18
10	2020	1009	1526	26.5	56.417	27.98	9.1	107.76	70.71	74.08	0.3	4.2	24	15
11	2021	115	2131	3.6	55.301	26.707	9.2	57.63	50.73	77.04	0.6	5.4	25	13
12	2021	117	250	14.9	55.252	26.705	17.9	260.57	42.27	67.37	1.1	4.5	22	25
13	2021	131	1604	34.2	56.904	28.12	9.0	82.61	64.34	56.31	0.5	4.9	19	19
14	2021	303	235	26.6	56.971	28.213	17.1	267.20	31.47	70.57	1.0	4.0	23	16
15	2021	303	316	5.6	56.947	28.254	18.4	107.97	68.19	64.02	0.5	4.0	22	16
16	2021	1010	1611	24	55.293	27.247	16.7	290.57	38.29	47.00	1.2	4.7	23	17
17	**2021**	**1114**	**1207**	**4.3**	**56.099**	**27.52**	**19.5**	**252.29**	**37.70**	**64.96**	**1.3**	**6.2**	**21**	**33**
18	2021	1114	1402	55.9	56.184	27.556	17.0	75.22	49.25	63.16	1.0	4.6	21	23
19	2021	1114	1522	19	56.171	27.492	13.8	89.87	52.84	64.59	1.0	4.3	23	18
20	2021	1114	1619	56.9	56.174	27.486	18.6	260.57	42.27	67.37	0.9	4.4	22	22
21	2021	1115	1336	12.2	56.185	27.563	17.4	257.43	37.70	64.96	0.8	5.0	23	28
22	2021	1115	1805	38.7	56.289	27.509	18.9	78.71	33.23	61.81	0.9	4.1	22	15
23	2021	1116	512	14.4	56.121	27.551	18.9	115.89	61.98	67.20	0.5	5.2	19	17
24	2021	1118	1610	43	56.133	27.504	15.2	264.48	36.59	32.98	0.9	4.3	23	12
25	2021	1119	1851	0	56.255	27.568	14.1	265.02	45.22	82.95	0.9	4.0	22	10
26	2021	1221	1636	12.3	56.225	27.549	18.0	90.74	34.78	42.19	0.4	4.6	44	23
27	2021	1227	731	56	56.272	27.578	15.3	292.36	35.53	53.95	0.4	5.0	10	28

Distribution of the stations has not perfect azimuthal coverage around the earthquakes epicenters. All of the aftershocks are located in north of MFF and seems to be related to MFF in this area. It seems that fault propagated fold of Gianu anticline (a segment of MFF) is responsible for the 2021 Fin second event. Possible explanations for far distance of the aftershocks to MFF are: 1) shift or drift of aftershocks, because of imperfect azimuthal coverage of both IGUT and IIEES stations, and 2) less dipping of the MFF in the epicentral area in comparison to the previous studies like Berberian (1995). He suggested ~45° dipping for MFF in this area. The situation of aftershocks has similarity to the 2006 Fin earthquake, in which the pattern of coseismic surface uplift is centered on the common limb of the Fin syncline and Guniz anticline in north of the epicentral area (Roustaei et al. 2010). Closer distance of the IGUT aftershocks cluster to MFF in comparison to of the IIEES could be related to less number and distant station spacing of IIEES network.

Mechanism of 27 earthquakes including 10 aftershocks with M_N magnitude greater than 4.0 was solved. This range of magnitude was chosen, because of having event enough energy and therefore good polarity especially in far stations. These events were processed using first P motion method. Mechanism of earthquakes was chosen based on number of the polarities, scattering of the stations on focal sphere, stability of the mechanism and local fault systems and geology of the area near the event. Stability of the mechanism depends on polarity of nodal planes boundary stations, degree of freedom of the nodal planes and diversity of the solutions, which are suggested by the software.

Mechanism of mainshock (12:07), #17, displays a reverse motion related to MFF with north dipping (37.7°) and W-E active plane and a small component of strike slip motion. This mechanism is in accordance to of the GCMT for this event, except dip value (85°). Our calculated dip for mainshock could justify far location of aftershocks cluster to Gianu anticline and MFF.

Mechanism of background seismicity is fairly associated with the related nearest fault system. Mechanism of events #5, 6, 10-15 shows dominant reverse mechanisms in accordance to the related local fault systems in their locations. Event #10 displayed a reverse mechanism related to HZF (NW-SE) with a small right lateral motion. Events #3, 5, 7, 9 and 16 are related to MFF, while event #1 is related to ZFF, both with ~E-W and north dipping active plane. They show dominant reverse mechanisms. Event # 2 related to MFF shows an odd mechanism. Earthquakes #11 and 12 are probability related to Qeshm island anticlines and faults. Aftershocks #18-22 amd # 25 have pure reverse mechanisms in accordance to the mainshock with active planes of north dipping E-W direction. Aftershocks #23-27 shows dominant reverse mechanisms both with ~NE-SW active planes not completely related to MFF. Events #8 are suspended to relate to MFF. Appendix 1 shows distribution of polarities on focal mechanism of the greatest background seismicity and aftershocks.

3.2- Geodynamic

Figure 3a displays pressure vectors of the focal mechanisms solved by GCMT and us. Black vectors were drawn for GCMT events. Blue, red and green vectors were drawn for background seismicity, second shock and aftershocks, respectively. Gray cross shows dominant orientation of all of the vectors. Inset histogram shows orientation of all of the vectors. Pressure direction in each area is approximately normal to fault system in this area. Direction of the gray cross is in accordance to direction of the velocity GPS station (Vernant et al. 2004) in ~60 km NNW (near Hajiabad in Fig. 1). Generally, pressure vectors of the focal mechanisms including background seismicity, the 2021 Fin mainshock and aftershocks is normal to local fault systems and geological structures (axes of anticline and syncline) of the area.

According to the fact that even small vertical displacements of the surface could be detectable in high resolution pictures (e.g. Nemati et al. 2020), therefore deformation in geomorphology were detected by comparing two sets of Sentinel-2 satellite pictures. In this prospecting, no mature rupture was detected in epicentral area of earthquakes. Only fractures, probability made by settlement following ground shaking and vertical ground motion of the earthquakes were seen in compacted area like road (Fig. 3b). Fig. 3c, d and e shows opening crack and rock falls following the 2021 Fin earthquakes in Bandar-e Abbas to Haji Abad main road (56.3°E and 27.7°N).

3.3- Statistics of aftershocks

Statistical parameters of aftershocks (Fig. 4) show fair quality of aftershocks recording by a regional seismological network (IGUT). During 50 days elapsed from mainshock, more than 95% of the 272 aftershocks with the M_N greater than 2.5 occurred in a small rectangle (0.25ºN×0.5ºE). Locating of boundary earthquakes (related to station distribution, inset map of Fig. 2) is not simple for the networks operators, because of azimuthal gap problem. Empirical relationships for area of aftershocks scattering in Iran ($Log_{10}(A)=0.25\ M_N+1.7$; Nemati 2014) for this earthquake was calculated about A=1778 km^2 (M_N is magnitude of the mainshock). The real value, which was achieved in this study (1378 km^2), is small in comparison to the calculated value (A). Scattering of the aftershocks in a small area related to magnitude of the mainshock maybe indicate to acceptable locating of earthquakes by IGUT network.

RMS error of majority of aftershocks in this sequence is less than 0.6s, which is acceptable for a regional network (Fig. 4a). Statistical analysis shows that approximately 30% of the aftershocks were located using more than 20 stations and 30 phases. Finally, 90% of aftershocks were located with azimuthal gap less than 180º (Fig. 4b). Fig. 4c displays scattering of aftershocks of various magnitudes with depth. This diagram shows that the greater aftershocks (M_N>3.5) occurred in intermediate depths. This indicates to a stronger crust in 10-20 km depth range, which is coincident to the bed rock under the sedimentary cover. Majority of aftershocks occurred in 5-20 km depth range (Fig. 4c). It shows that sedimentary cover in this part of Zagros is still seismogen. Four aftershocks with M_N magnitude greater than 4.5 and 14 aftershocks with M_N greater than 4.1 occurred in this sequence.

Figure 4d displays history of ruptured area for the earthquakes. A-B line has been shown in the Fig. 2 and all of the events nearer than 50 km to the A-B line were projected to the special and temporal diagram. Ellipses show previous large earthquakes and their sequences and black thick line shows ruptured area of the 2021 event based on the IGUT aftershocks. Four large earthquakes with M_N greater than 5.1 (a-d in Fig. 4d) occurred in epicentral area of the 2021 Fin earthquake during the last 16 years. They ruptured parts of this area previously. Although, no earthquake greater than 2.0 occurred in epicentral area from one month before occurrence the 2021 earthquakes, no considerable seismic gap is seen in diagram. Normal background seismicity could be seen in the history diagram. Notwithstanding the eastern Iran earthquakes with significant seismic gaps (e.g. Savidge et al. 2020, Nemati et al. 2020), in this area of Zagros, normal background seismicity occurred before the earthquake in this area rather than occurring a considerable seismic gap. A possible explanation for this phenomena could be the fact that general b-value for Zagros is obviously greater than of the eastern Iran (e.g. Nemati 2019).

3.4- Strong motion analysis

Figure 5 (a) and (b) shows iso-acceleration maps of the mainshocks and Fig. 5c, d compare the two accelerograms in north and south of the epicenter of the mainshocks. The maps show that in both earthquakes, the Siahoo station recorded maximum PGA amng the other stations. The comparison is between Siahoo and Bandar-e Abbas-1 acceleromety stations in ~30 km and ~50 km northeast and southeast of the 12:07 earthquake, respectively. As seen in Fig. 5c, frequency and amplitude of the Siahoo station (black waveform) in northeast are much greater than of the station in southeast (orange waveform). Amplitude of waveform of the northeast station is >250 cm/s^2, while this parameters for waveform of the southeast station is <100 cm/s^2. Also, duration of the recorded waveform in northeast station is ~10s shorter than of the southeast station. Duration of waveforms is usually defined the time window from the beginning to where the amplitude damps to 0.1 of the maximum. If strike of coseismic rupture is near ENE-WSW direction, it could be concluded that the rupture was propagated from the south to the north, unilaterally.

Figure 5d shows the comparison between Siahoo and Qale Qazi acceleromety stations in ~30 km northeast and southeast of the 12:08 earthquake, respectively. Frequency and amplitude of the Siahoo station (black waveform) in northeast are much greater than of the station in southeast (orange waveform). Amplitude of waveform of the northeast station is >250 cm/s^2, while this parameters for waveform of the southeast station is <80 cm/s^2. Also, duration of the recorded waveform in northeast station is ~5s shorter than of the southeast station. If MFF segment related to Gianu anticline is supposed as causative fault for the second mainshock, it could be concluded that the rupture was propagated from the south to the north, unilaterally.

The strike and length of coseismic rupture of the second shock could be estimated from distribution and elongation of aftershocks recorded by IGUT and IIEES seismological networks. This is preliminary estimation, which could be reasonable (e.g. Nemati 2015). The strike of the rupture associated to aftershocks distribution could be in ~E-W to ENE-WSW direction. Also, strike of MFF segment related to the earthquakes is ENE-WSW. Length of coseismic rupture associated to aftershocks elongation could be ~50 km. If we accept northward unilateral directivity and northward dipping of the MFF as causative fault of the second mainshock, it might be concluded that the rupture was propagated from shallow depth to deep area of the fault along N-S direction (from 10 km hypocenter toward 13 km centroid). Comparison of the 12:07 earthquake waveforms was not possible for the same stations as 12:08 shock, because the data of accelerations has not been released by the BHRC, for the Qaleh Qazi station. It could be concluded that causative faults of the shocks are back thrust, because, rupture propagation of the 12:07 event from south to north means that it propagated from depth to surface (from 20 km hypocenter toward 12 km centroid) along N-S direction.

3.4- Coulomb analysis

In order to investigate the phenomenon of interaction between the 2021 Fin seismic sequences, firstly, the change of seismic stress caused by the first earthquake (reference fault) has been done by considering the second earthquake as the receiving fault. In Coulomb stress change calculations, areas with warm colors indicate the range of increase in stress and areas with cold colors indicate a decrease in stress (Fig. 6). Then, impression of the second shock on the aftershocks was investigated. Position and geometric parameters of the analyzed earthquakes with Coulomb method were listed in table (2).

Table 2
Position and geometric parameters of the faults causing the Finn earthquake pair. Longitude, latitude and depth of the events were adopted from IGUT and Strike, dip and rake of them were adapted from this study and GCMT, respectively.

Event	(E°)Long.	(N°). Lat	(°)Strike	(°)Dip.	(°)Rake	(km) Depth
14/11/2021_12:07:04	56.084	27.556	252.29	37.70	64.96	19.5
14/11/2021_12:08:38	56.174	27.536	275	66	98	10.0

Figure 6 (a) shows Coulomb stress map of the mainshock-1, while figure 6 (b) displays Coulomb stress areas of the mainshock-2. Fault normal and fault parallel section lines were shown in both maps. Depth sections for the two mainshocks in fault normal (A-B) and fault parallel (C-D) directions were shown in Fig. 6c. According to the Fig. 6a, the asterisk, which shows hypocenter of the second mainshock, is located in increasing stress area (red area) resulted by the mainshock-1. The small green line (fault trace of the first shock, predicted by the Coulomb software) is exactly coincident with MFF segment in south of hypocentral area, which is not accidental. Dip of the coseismic fault of the first shock is assumed 37.5 NNW, which is adapted from the archived source parameters in this paper. Majority of aftershocks (small green dots) occurred in area of increasing stress produced by second shock. Indeed, the aftershocks belong to the mainshock-2 and therefore, occurred on increasing stress area (red area) of the mainshock-2 (Fig. 6b). The bigger yellow circles are the aftershocks and background seismicity of the table 1. In fault normal section (A-B), depth rupture areas for the two shocks are seen. They are in blue area and it means that the shocks discharged seismic stress in the ruptured areas. Fig. 6c also shows distribution of aftershocks related to the stress areas in depth.

To better display of the events in depth, two distinct sets of earthquakes were shown in sections. Small green dots in section A-B and C-D show earthquakes of the table 1 and all of aftershocks, respectively.

Discussion And Conclusions

The epicentral area of the aftershocks in closer view shows that IGUT network has been recorded aftershocks in better quality and quantity than of the IIEES. But the two regional networks help this idea that the mountain frontal fault is probability recognized as cause for the second earthquake.

All of the aftershocks are located in north of MFF and seems to be related to MFF in this area. According to calculated reverse mechanism with north dipping ~E-W plane in this paper, it seems that fault propagated fold of Gianu anticline (lying on a segment of MFF) is responsible for the 2021 Fin event. It is exactly similar to the 2006 Fin earthquake of 6.4, in which fault propagated fold of Guniz anticline (lying on a segment of MFF) is responsible for the 2006 Fin event. It is common in the Zagros simply folded belt.

Mechanism of earthquakes and the greater aftershocks mainly shows dominant reverse mechanisms, fairly in accordance to the related local fault systems in their locations. In epicentral area, most of aftershocks displays reverse mechanisms with ~E-W northward dipping active plane. To the east, the strike of active plane in the mechanism of background seismicity changes from ~E-W to ~NW-SE direction, because of existence of ~NW-SE High Zagros, Main Zagros Reverse Faults and Zendan-Minab strike slip fault systems.

Pressure direction for each individual earthquake, concluded from focal mechanism solution, is approximately normal to fault system in related area. Dominant orientation of the pressure vectors of the focal mechanisms solved by GCMT and this study shows ~15° NNE-SSW direction. Direction of this orientation is in accordance to direction of the velocity GPS station in north of the area.

Statistical parameters of aftershocks show fair quality of aftershocks recording in 50 days after the earthquakes by a regional seismological network (IGUT). The real area of scattering of aftershocks, which was achieved in this study, is small in comparison to the calculated value using empirical relationships between magnitude of the mainshocks and aftershocks area of scattering. Scattering of the aftershocks in a small area related to magnitude of the mainshock maybe indicate to acceptable locating of earthquakes in IGUT network, because locating of boundary earthquakes is not simple for the networks operators, because of azimuthal gap problem.

Majority of the aftershocks were located with azimuthal gap less than 180º and using acceptable number of stations and phases, therefore RMS error of majority of aftershocks is acceptable for a regional network. The greater aftershocks (M_N>3.5) occurred in intermediate depths, indicating a stronger crust in 10-20 km depth range, which is coincident to the bed rock under the sedimentary cover in Zagros. Depth range of aftershock occurrence shows that sedimentary cover in this part of Zagros is still seismogen.

Four large earthquakes occurred in epicentral area of the 2021 Fin earthquake during the last 16 years, which is not abnormal for Zagros. They ruptured parts of Fin epicentral area previously. No specific seismic gap is seen before the earthquakes in investigated area. The earthquakes of eastern Iran are usually associated with significant seismic gaps. For example, the 1968 Dasht-e Bayaz, the 1997 Abiz and the 1981 Golbaf earthquakes occurred after obvious and considerable seismic gaps. In this area of Zagros, normal background seismicity occurred before the earthquakes. Maybe the reason is that b-value for Zagros is generally larger than of the eastern Iran.

Comparison between accelerograms of the northeast and southern stations of the 12:07 earthquake epicenter indicates that, frequency and amplitude of the northeast stations are much greater than of the station in south. Also, duration of the recorded waveform in northeast station is shorter than of the south station. Also, comparison between stations in northeast and southeast of the 12:08 earthquake indicates that frequency and amplitude of the station in northeast are much greater than of the station in southeast. Also, duration of the recorded waveform in northeast station is shorter than of the southeast station. Strike of the coseismic rupture is estimated near ENE-WSW direction. It could be concluded that both ruptures was propagated from the south to the north, unilaterally.

The strike and length of coseismic rupture could be estimated from distribution and elongation of aftershocks recorded by reliable seismological networks. This is preliminary estimation, which could be reasonable. The strike of the rupture associated to aftershocks distribution could be in ~E-W to ENE-WSW direction (associated to MFF). Depth dimension of coseismic rupture of the second event using both aftershocks elongation and special and temporal diagram is estimated ~50 km. Northward dipping of the MFF as causative fault of the second mainshock maybe result that the rupture of the 12:08 event was propagated from shallow depth to deep area (from 10 to 13 km depth, from hypocenter toward centroid) of the fault along N-S direction. If causative fault of the first shock is a back thrust with opposite dipping relative to the second shock, it might be concluded that the rupture was propagated from depth to surface (from 20 to 12 km depth, from hypocenter toward centroid) of the fault along N-S direction.

Increase in seismic activity is usually observed in areas with positive values of Coulomb stress change. Stress increase area of the first shock is manifested as approximately a symmetric pattern relative to the rupture plate. Symmetric and asymmetric patterns of coulomb stress are usually seen in pure dip slip and strike slip events, respectively. It is not surprising, because patterns of wave propagation in the two kinds of events are different. Stress map of the first shock is more symmetric in comparison to of the second shock. A possible explanation for this natural phenomenon could be the fact that the second shock occurred in a much more disturbed environment than the first shock.

Coulomb analysis indicates that the second event occurred in a very short time and close space from the first shock, because the first shock changes seismic stress in the epicentral area, highly and rapidly.

Mechanism solutions of the mainshock-2 could be questionable, because close origin time of the two shocks with large magnitude could destroy the waveforms of the second shock. Mechanism of the mainshock-2 could not be solved using the first P motion method, because waves of the first shock covered waves of the mainshock-2, completely. Using the GCMT dip for mainshock-2 in calculations, it results a fault trace on surface in northern area related to of the first shock and MFF. This is not in accordance with the geology. The geological maps does not show any fault in this area.

Another conclusion could be taken from hypocentral depths released by IGUT for the mainshocks (20 and 10 km, respectively), centroid depths reported by GCMT (12 and 13 km, respectively) and directivity. Northward directivity, which was obviously seen, is reliable for the two mainshocks. Therefore, the rupture of the second shock may propagate from the south to north and from shallow (10 km hypocenter) toward depth (13 km centroid) of the north dipping causative fault. If we accept these sets of data, the first shock may happened in a south dipping fault and originated in 20 km (hypocenter) and propagated to the shallow depth of 12 km (centroid).

References

1. Alavi M (2004) Regional stratigraphy of the Zagros fold-thrust belt of Iran and its proforeland evolution. Am J Sci 304:1–20
2. Bachmanov DM, Trifonov VG, Hessami KT, Kozhurin AI, Ivanova TP, Rogozhin EA, Hademi MC, Jamali FH (2004) Active faults in the Zagros and central Iran. Tectonophysics 380:221–241
3. Berberian M (1995) Master ‘Blind’ thrust faults hidden under the Zagros folds: active basement tectonics and surface morphotectonics. Tectonophysics 241:193–224
4. Walker RT, Andalibi MJ, Gheitanchi MR, Jackson JA, Karegar S, Priestley K (2005) Seismological and field observations from the 6 November 1990 Furg (Hormozgan) earthquake: a rare case of surface rupture in the Zagros mountains of Iran. Geophys J Int 163:567–579
5. Harris RA (1998) Introduction to special section: Stress triggers, stress shadows, and implications for seismic hazard. Journal of Geophysical Research: Solid Earth 103(B10):24347–24358
6. Hatzfeld D et al (2010) The kinematics of the Zagros Mountains (Iran). Geological Society, London, Special Publications, doi:10.1144/SP330.3; 330: 19-42
7. Lin J, Stein RS (2004) Stress triggering in thrust and subduction earthquakes, and stress interaction between the southern San Andreas and nearby thrust and strike-slip faults. J. Geophys. Res. 109, B02303 (2004), doi: 10.1029/2003JB002607
8. King GCP, Cocco M (2001) Fault interaction by elastic stress changes: New clues from earthquake sequences. Advances in geophysics, vol 44. Elsevier, pp 1–VIII
9. Mcquarrie N (2004) Crustal scale geometry of the Zagros fold–thrust belt, Iran. J Struct Geol 26:519–535
10. Nemati M, Hatzfeld D, Gheitanchi M, Sadidkhouy A, Mirzaei N (2011) Microseismicity and seismotectonics of the Firouzkuh and Astaneh faults (east Alborz, Iran). Tectonophysics 506:11–21
11. Nemati M (2014) An appraisal of aftershocks behavior for large earthquakes in Persia. Journal of Asian Earth Science 79:432–440
12. Nemati M (2015) Slip distribution, aftershocks and co-seismic fault of some large Persian earthquakes. Environmental Earth Science 73(11):7165–7181
13. Nemati M (2019) Inter-event times between large earthquakes in Iran. Earthquake Sciences. doi: 10.29382/eqs-2019-0000-00
14. Nemati M, Jafari Hajati F, Rashidi A, Hassan-zadeh R (2020) Seismology of the 2017 Hojedk earthquakes (M_N 6.0- 6.1), Kerman province, SE Iran. Tectonophysics 780:228398
15. Nissen E, Ghods A, Karasözen E, Elliott JR, Barnhart WD, Bergman EA, Hayes GP, Jamal-Reyhani M, Nemati M, Tan F, Abdulnaby W, Benz HM, Shahvar MP, Talebian M, Chen L (2019) The 12 November 2017 Mw 7.3 Ezgeleh–Sarpolzahab (Iran), Eearthquake and active tectonics of the Lurestan arc 2. JGR-Solid Earth. 10.1029/2018JB016221
16. Okada Y (1992) Internal deformation due to shear and tensile faults in a half-space. Bull Seismol Soc Am 82(2):1018–1040

17. Ottemöller L, Havskov J (2012) The earthquake analysis of SEISAN software, version 9.1, http://www.geo.uib.no/Seismologi/SOFTWARE/SEISAN_9.1, 2022
18. Roustaei M, Nissen E, Abbassi M, Gholamzadeh A, Ghorashi M, Tatar M, Yamini-Fard F, Bergman E, Jackson J, Parsons B (2010) The 2006 March 25 Fin earthquakes (Iran)—insights into the vertical extents of faulting in the Zagros Simply Folded Belt. Geophys J Int 181:1275–1291
19. Savidge E, Nissen E, Nemati M, Karas¨ozen E, Hollingsworth J, Talebian M, Bergman E, Ghods A, Ghorashi M, Kosari E, Rashidi A, Rashidi A (2019) The December 2017 Hojedk (Iran) earthquake triplet - sequential rupture of shallow reverse faults in a strike-slip restraining bend. Geophys J Inter 217(2):909–925
20. Stein RS (1999) The role of stress transfer in earthquake occurrence. Nature 402(6762):605–609
21. Talebian M, Jackson J (2004) A reappraisal of earthquake focal mechanisms and active shortening in the Zagros mountains of Iran. Geophys J Int 156:506–526
22. Tatar M, Hatzfeld D, Ghafoury-Ashtiani M (2004) Tectonics of the Central Zagros (Iran) deduced from microearthquake seismicity. Geophys J Int 156:255–266
23. Toda S, Stein RS, Richards-Dinger K, Bozkurt SB (2005) Forecasting the evolution of seismicity in southern California: Animations built on earthquake stress transfer. Journal of Geophysical Research: Solid Earth 110:B5
24. Vernant P, Nilforoushan F, Hatzfeld D, Abassi M, Vigny C, Masson F, Nankali H, Martinod J, Ashtiani A, Bayer R, Tavakoli F, Che´ry J (2004) Contemporary crustal deformation and plate kinematics in Middle East constrained by GPS measurements in Iran and northern Oman. Geophys J Int 157:381–398
25. Wessel P, Smith WHF (1998) New improved version of Generic Mapping Tools released. EOS Trans AGU 79:579
26. Yamini-Fard F, Hatzfeld D, Farahbod AM, Paul A, Mokhtari M (2007) The diffuse transition between the Zagros continental collision and the Makran oceanic subduction (Iran): microearthquake seismicity and crustal structure. Geophys J Int 170:182–194
27. Yazdanfar C, Nemati M, Agh Ataby M, Roustaei M, Nilfouroushan F (2018) Stress transfer, aftershocks distribution and InSAR analysis of the 2005 Dahuieh earthquake, SE Iran. Journal of African Earth Science 147:211–219

Figures

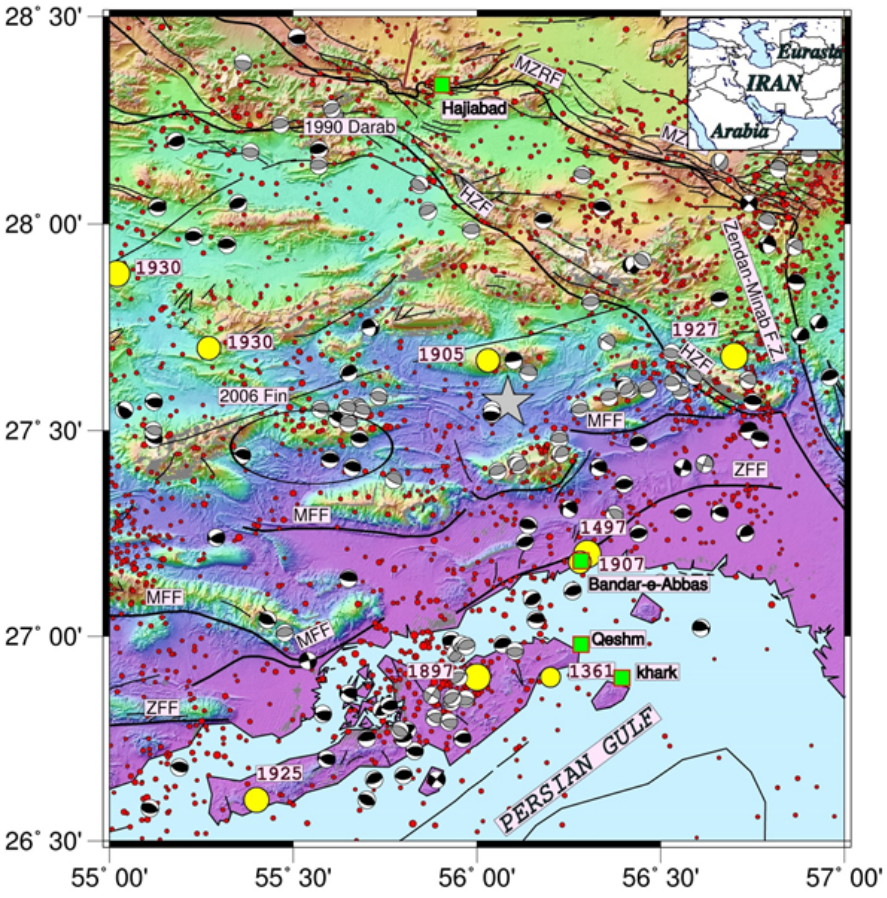

Figure 1

Seismotectonic map of the 2021 Fin earthquakes and the neighboring area. Black and gray focals show GCMT and Nissen et al. (2019) mechanisms in Zagros, respectively. Red and Yellow circles display background seismicity and historical earthquakes, respectively. Asterisk shows the 2021 Fin mainshocks locations (IGUT).

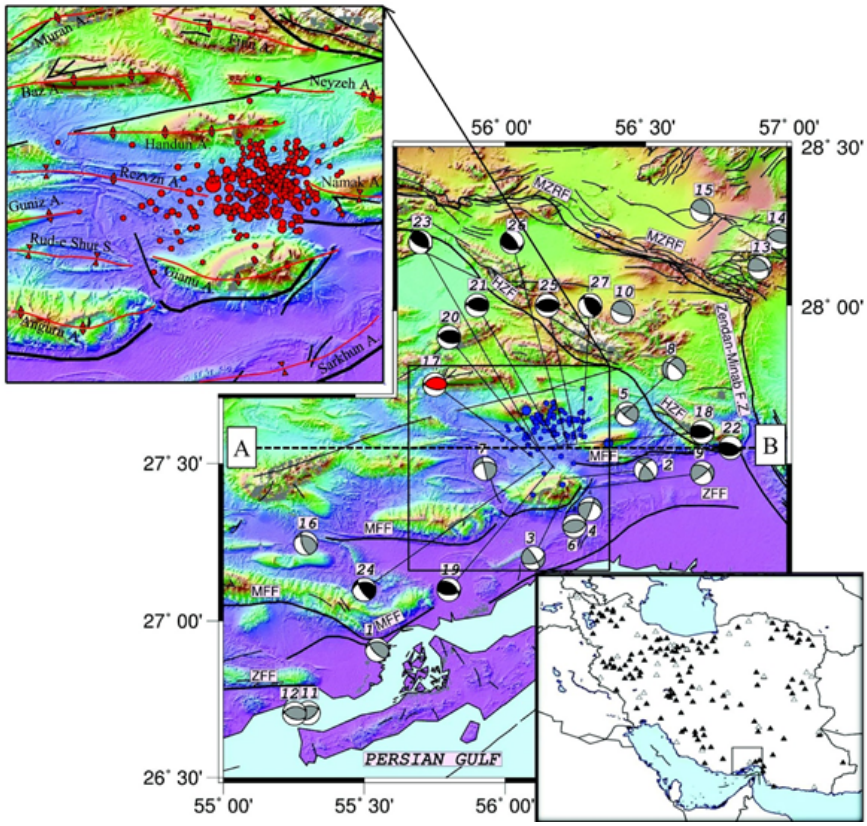

Figure 2

Distribution 272 aftershocks and mechanisms of the greatest ones. Gray, red and black circles display mechanisms of mainshock, background seismicity and aftershocks, respectively. A-B is section line of the Fig. 4e.

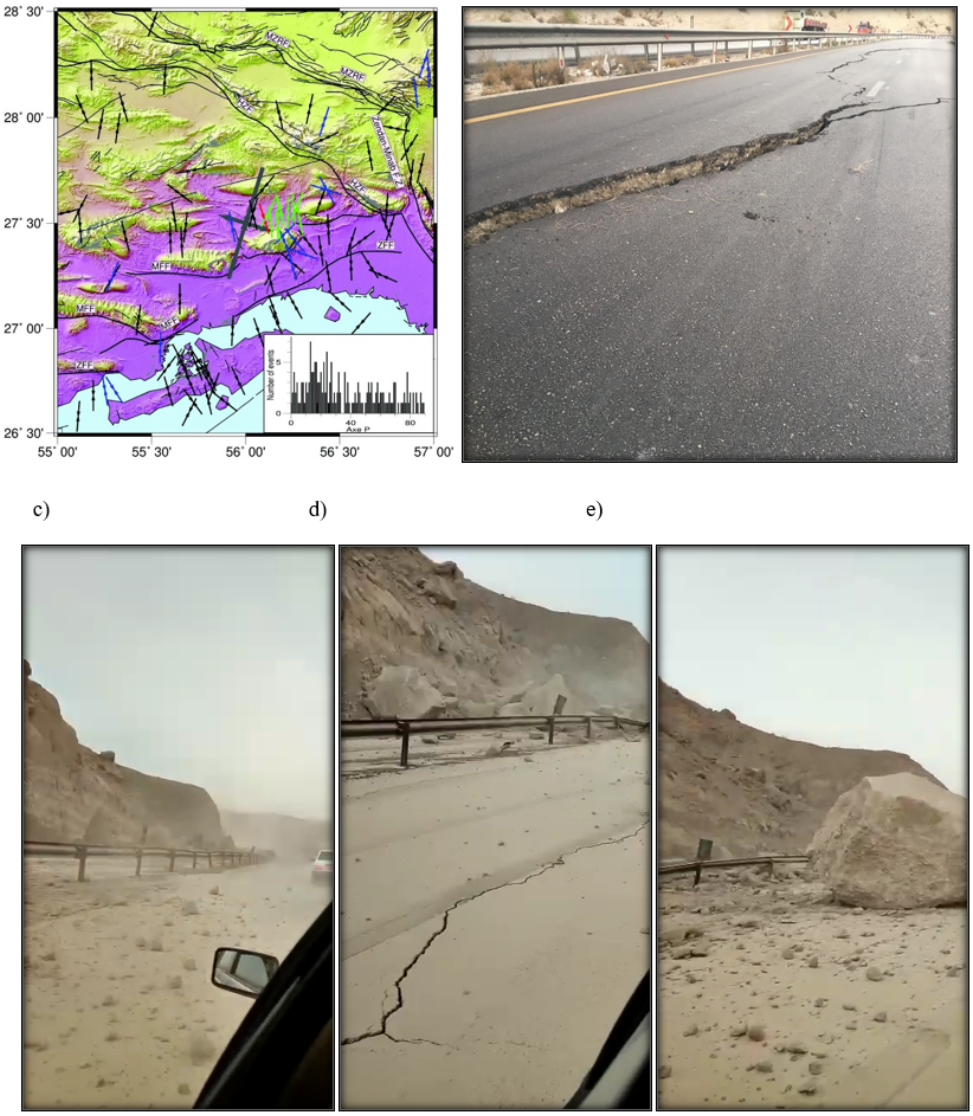

Figure 3

a) Pressure vector of GCMT and calculated mechanisms in epicentral area. Inset histogram shows dominant orientation of the vectors. Red, green, blue and black vectors indicate to the 2021 Fin mainshock, aftershocks, background seismicity solved in this study and GCMT solved background seismicity, respectively, b) opening a fracture in road, c, d and e) crack and rock falls following the 2021 Fin earthquakes. Pictures were taken at 56.3°E and 27.7°N coordinate.

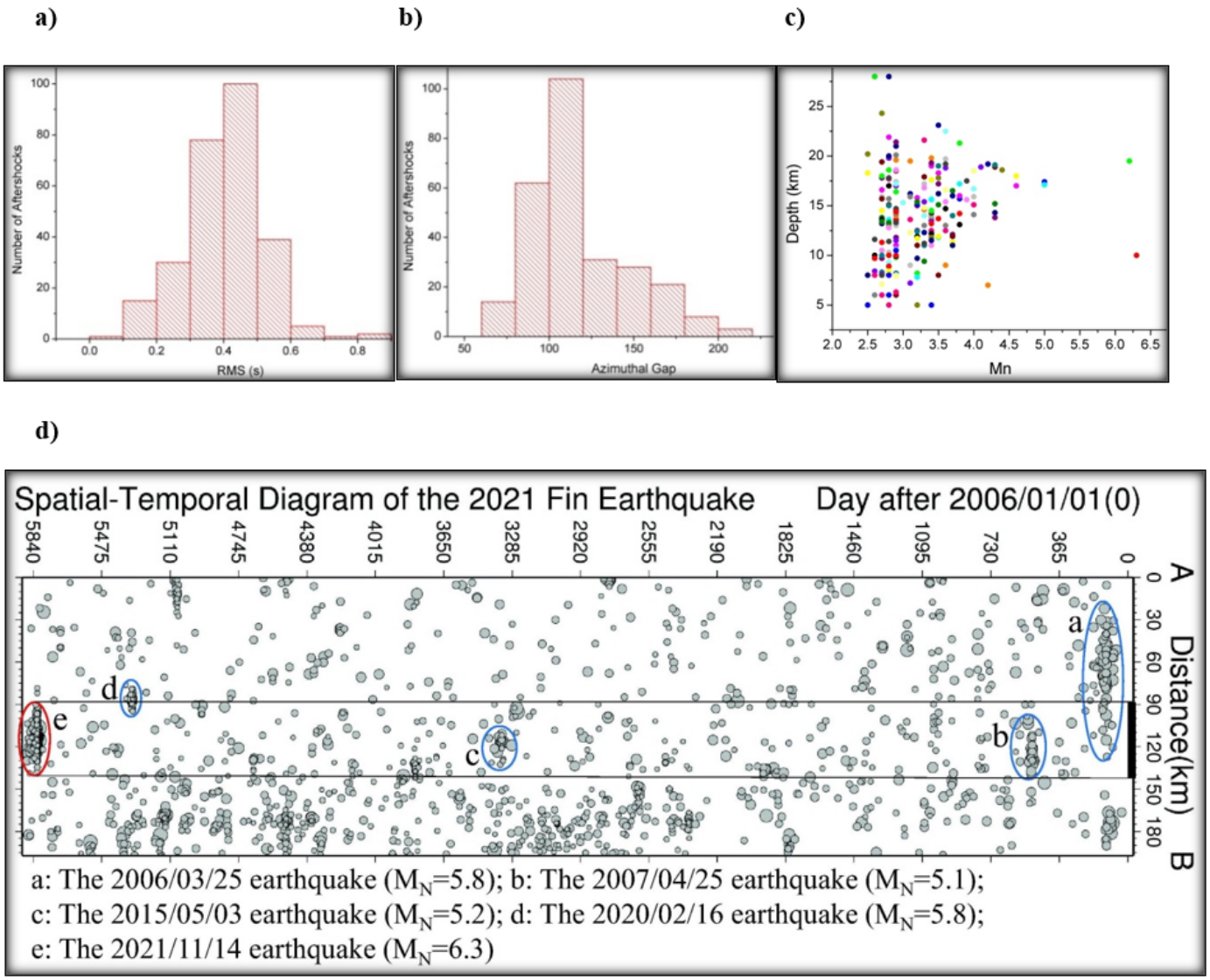

Figure 4

Some important statistical parameters. a) RMS, b) azimuthal gap and c) magnitude- depth diagram of the aftershocks. d) History of ruptured area and the neighboring.

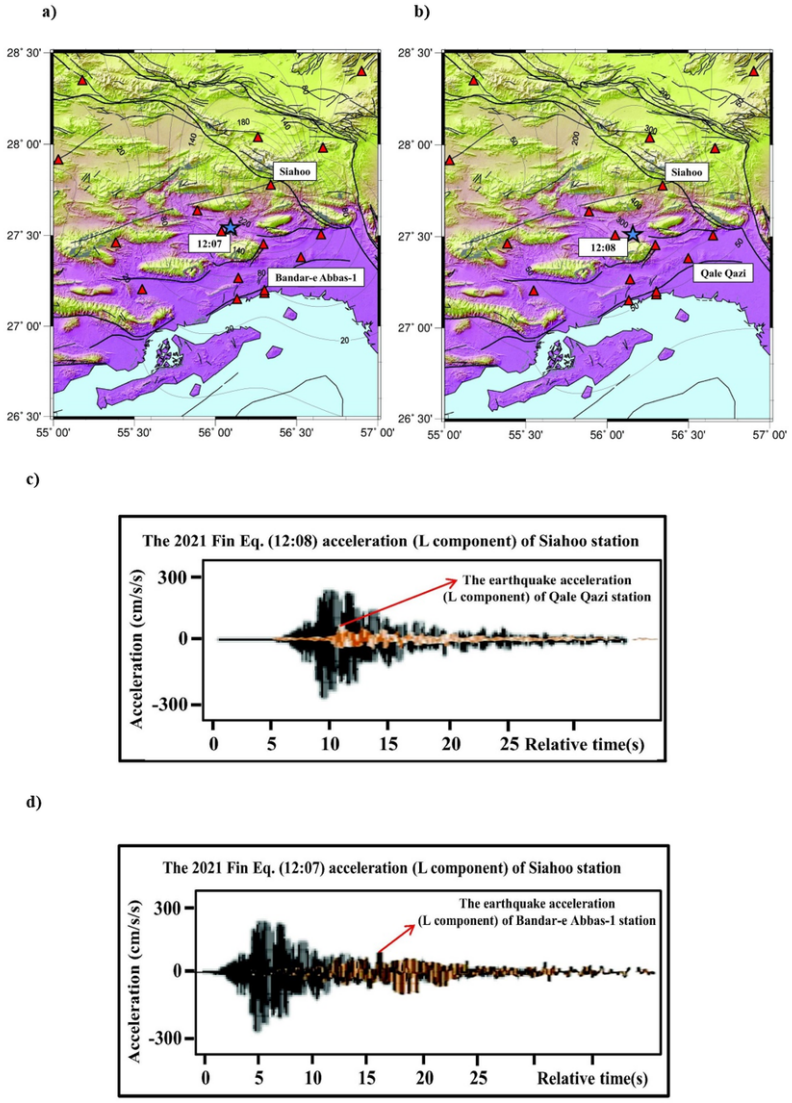

Figure 5

Iso-acceleration maps of the mainshocks. a) 12:07, b) 12:08 and c) comparisons of the two accelerograms in north and south of the epicenter of the first (c) and second (d) mainshocks. Asterisk in (a) and (b) maps show epicenters of the mainshocks. Triangles show BHRC accelerometer stations.

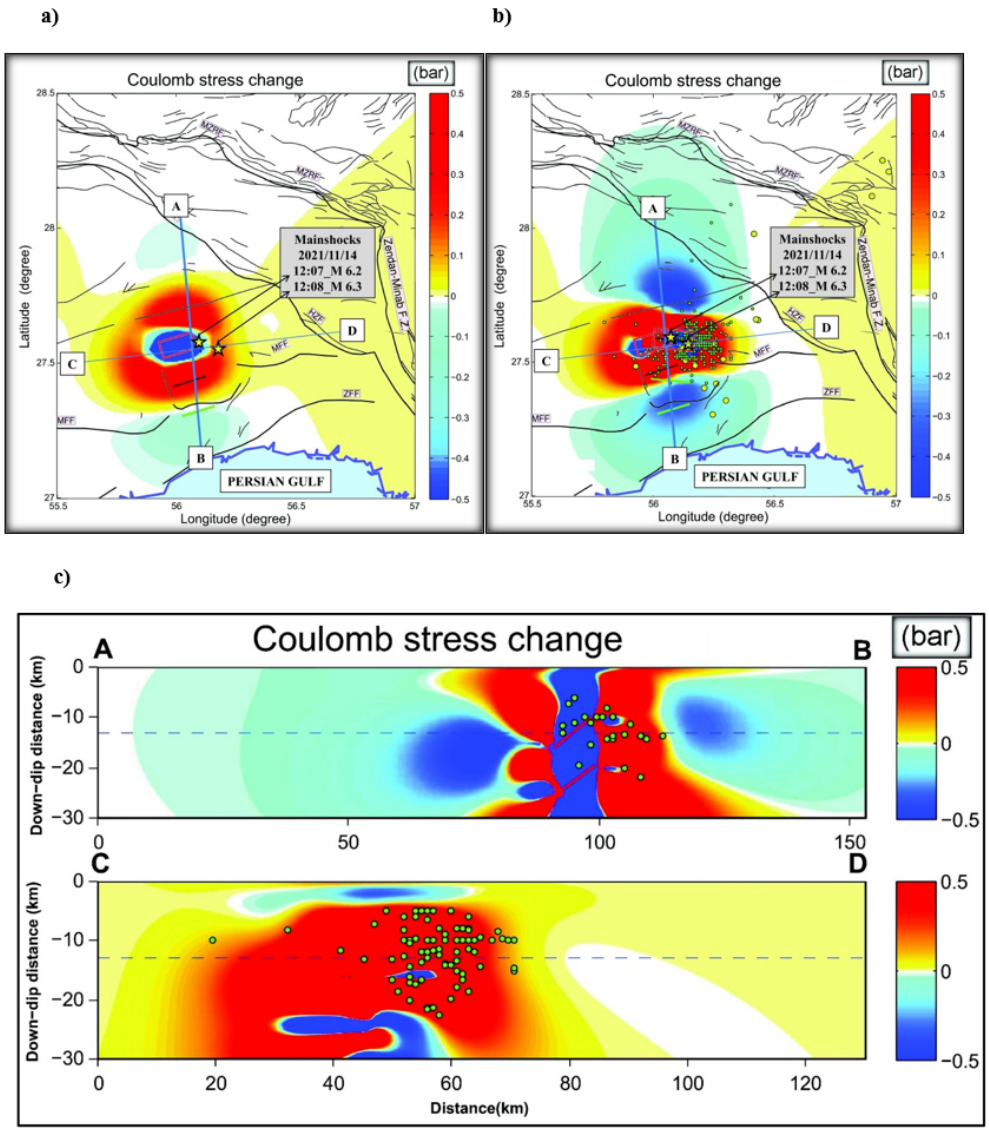

Figure 6

Coulomb stress map of the mainshocks (a) and (b). c) Depth sections in fault normal (A-B) and fault parallel (C-D) directions.

Supplementary Files

This is a list of supplementary files associated with this preprint. Click to download.

- Appendix.docx